PAPER

High-pressure synthesis and spin glass behavior of a Mn/Ir disordered quadruple perovskite $CaCu_3Mn_2Ir_2O_{12}$

IOP Publishing Journal of Physics: Condensed Matter
J. Phys.: Condens. Matter **32** (2020) 075701 (6pp) https://doi.org/10.1088/1361-648X/ab5386

High-pressure synthesis and spin glass behavior of a Mn/Ir disordered quadruple perovskite $CaCu_3Mn_2Ir_2O_{12}$

Xubin Ye[1,2], Zhehong Liu[1,2], Weipeng Wang[1,2], Zhiwei Hu[3], Hong-Ji Lin[4], Shih-Chang Weng[4], Chien-Te Chen[4], Richeng Yu[1,2], Liu-Hao Tjeng[3] and Youwen Long[1,2,5]

[1] Beijing National Laboratory for Condensed Matter Physics, Institute of Physics, Chinese Academy of Sciences, Beijing 100190, People's Republic of China
[2] School of Physical Sciences, University of Chinese Academy of Sciences, Beijing 100049, People's Republic of China
[3] Max Planck Institute for Chemical Physics of Solids, Dresden 01187, Germany
[4] National Synchrotron Radiation Research Center, Hsinchu 30076, Taiwan, Republic of China
[5] Songshan Lake Materials Laboratory, Dongguan, Guangdong 523808, People's Republic of China

E-mail: ywlong@iphy.ac.cn

Received 30 July 2019, revised 16 October 2019
Accepted for publication 1 November 2019
Published 18 November 2019

Abstract

A new 3*d*-5*d* hybridized quadruple perovskite oxide, $CaCu_3Mn_2Ir_2O_{12}$, was synthesized by high-pressure and high-temperature methods. The Rietveld structure analysis reveals that the compound crystallizes in an $AA'_3B_4O_{12}$-type perovskite structure with space group *Im*-3, where the Ca and Cu are 1:3 ordered at fixed atomic positions. At the B site the 3*d* Mn and the 5*d* Ir ions are disorderly distributed due to the rare equal +4 charge states for both of them as determined by x-ray absorption spectroscopy. The competing antiferromagnetic and ferromagnetic interactions among Cu^{2+}, Mn^{4+}, and Ir^{4+} ions give rise to spin glass behavior, which follows a conventional dynamical slowing down model.

Keywords: high-pressure synthesis, quadruple perovskite oxide, spin glass

(Some figures may appear in colour only in the online journal)

1. Introduction

The compounds with ABO_3 perovskite structure composed of a 3D framework of corner-sharing BO_6 octahedra have attracted much attention, due to their large varieties of physical and chemical properties [1–5]. Chemical substitution either at *A* or *B* site is an effective method to tune the structure and physical properties of perovskites. For example, the *A*-site alkaline earth substitution for rare earth in manganates $La_{1-x}A_xMnO_3$ leads to insulator-to-metal and paramagnetism-to-ferromagnetism transitions [6–10]. The *B*-site substitution of Fe^{4+} by Co^{4+} in $SrFe_{1-x}Co_xO_3$ causes a series of magnetic transitions [11]. Specifically, as the *x* increases, the magnetic ground state changes from helimagnetic antiferromagnetic (AFM) state through cluster glass to ferromagnetic (FM) state with a high Curie temperature. In particular, if three quarters of *A* site in a simple ABO_3 is substituted by a transition metal ion *A*′, one may obtain an *A*-site ordered quadruple perovskite with the chemical formula of $AA'_3B_4O_{12}$ [12–16]. Since the ionic size of a transition metal is much less than that of a typical *A*-site cation such as alkaline, alkaline earth or rare earth metal, to sustain the perovskite structure, square-coordinated $A'O_4$ units and heavily tilted BO_6 octahedra show up in $AA'_3B_4O_{12}$, as presented in figure 1(a). The peculiar coordination environment of *A*′ site is favorable to accommodate a Jahn-Teller distortion ion like Mn^{3+} or Cu^{2+}. As a Cu^{2+} ion with $3d^9$ configuration is concerned, this square coordination may result in a d_{xy} hole state with the Cu–O square planar oxygen bond pointing between *x* and *y* [17]. The electronic states of Cu^{2+} can exhibit either localized or itinerant behavior depending on

the electronic properties of the *B*-site ions. Moreover, the *A′*-site Cu^{2+} spins can form a magnetic lattice with face-centered cubic symmetry. The direct-exchange interactions between the nearest neighboring Cu^{2+} ions compete with the superexchange interactions caused by Cu–O–*B* pathways, leading to unusual magnetic instability and even a magnetic tri-critical point [18–20].

$CaCu_3Mn_4O_{12}$ and $CaCu_3Ir_4O_{12}$ are two interesting examples in *A*-site ordered quadruple perovskite family. The former shows a large low-field magnetoresistance response with the absence of Mn^{3+}–O–Mn^{4+} double-exchange interactions, since only a single Mn^{4+} valence state occurs at the *B* site [21]. The later displays heavy Fermion behavior since the d_{xy} orbital of the Cu^{2+} strongly hybridizes with the Ir 5*d* orbitals via the O-*p* orbitals, so that the local moments of the Cu are incorporated in the itinerant 5*d* electrons of the Ir [22]. This coupling leads to the disappearance of long-range magnetic ordering of Cu^{2+} ions and strongly enhanced electronic specific heat. Recently, a few $AA'_3B_2B'_2O_{12}$-type quadruple perovskites with orderly distributed 3*d*/5*d* transition metals at the *B*/*B′* sites have been discovered [23–25]. One finds that the introduction of 5*d* electrons can significantly change the magnetic and electrical transport properties. On account of the interesting properties of $CaCu_3Mn_4O_{12}$ and $CaCu_3Ir_4O_{12}$, in this study, we prepare a 3*d*-Mn and 5*d*-Ir hybridized quadruple perovskite oxide $CaCu_3Mn_2Ir_2O_{12}$ (CCMIO) by using high pressure and high temperature conditions. The crystal structure, charge state, magnetism and electrical transport properties are studied in detail.

2. Experiment details

The compound of $CaCu_3Mn_2Ir_2O_{12}$ was synthesized as black polycrystalline powders. Highly pure (>99.9%) CaO, CuO, MnO and Ir powders with a 1:3:2:2 mole ratio were used as starting materials, and excess $KClO_4$ was applied as an oxidizing agent. These reagents were thoroughly mixed in an agate mortar within an argon-filled glovebox, and then sealed into a platinum capsule with 4.0 mm in diameter and length. The capsule was treated at 5.5 GPa and 1673–1773 K for 60 min on a cubic anvil-type high-pressure apparatus. The sample was quenched to room temperature (RT) once the heat treatment was finished, and then the pressure was gradually released. The product was washed using deionized water to exclude the residual KCl. In addition, $CaCu_3Ti_4O_{12}$ was prepared as described in [26], and Cu_2O single crystal was purchased from MaTeck-Material-Tenchnologie & Kristalle GmbH. These two oxides were used as x-ray absorption references.

The sample quality and crystal structure were identified by powder x-ray diffraction (XRD) on a Huber diffractometer with Cu $K_{\alpha 1}$ radiation ($\lambda = 1.5406$ Å). The diffraction angle (2θ) varies from 10 to 100° with 0.005° per step. The selected area electron diffraction (SAED) was performed at RT along [1 1 0] zone axis by a Philips-CM200 transmission electron microscope with a field emission gun operated at 200 keV. The structure refinement was performed by the Rietveld method using the GSAS program [27]. Soft x-ray absorption spectroscopy (XAS) measurements of Cu-$L_{2,3}$ and Mn-$L_{2,3}$ edges were carried out at beamline BL11A of the National Synchrotron Radiation Research Center (NSRRC) in Taiwan using the total electron yield mode. The Ir-L_3 spectra were measured at beamline BL07A of the NSRRC in transmission geometry. The field dependence of the isothermal magnetization (*M*) and temperature-dependent dc magnetic susceptibility (χ_{dc}) were measured using a commercial superconducting quantum interference device magnetometer (MPMS3, Quantum Design). The temperature dependence of the ac magnetization (*M′*) and electrical transport were measured on a physical property measurement system (PPMS7, Quantum Design).

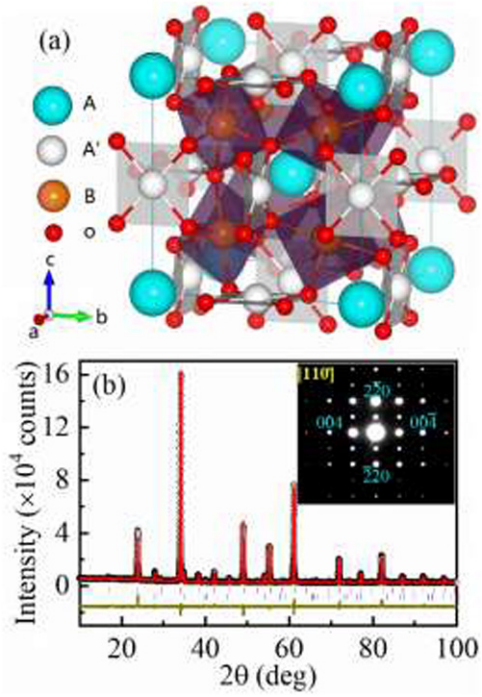

Figure 1. (a) Crystal structure of *A*-site ordered quadruple perovskite $AA'_3B_4O_{12}$ with space group *Im*-3. (b) XRD pattern and Rietveld refinement result for $CaCu_3Mn_2Ir_2O_{12}$. Observed (black circle), calculated (red line) and difference (dark yellow line) values are shown together with the allowed Bragg reflection (above ticks). The lower ticks present a small amount of impurity phase IrO_2 (~4.9 wt%). The inset in panel b shows a SAED pattern along the [1 1 0] zone axis.

3. Results and discussions

The crystal structure of CCMIO was characterized by powder XRD at RT. Figure 1(b) shows the XRD pattern as well as the structure refinement result. The Rietveld analysis shows that the compound possesses an *A*-site ordered perovskite structure with space group *Im*-3. It means that the Ca and Cu are 1:3 ordered at the *A* and *A′* sites, respectively, whereas the Mn and Ir are randomly distributed at the *B* site. To confirm the Mn/Ir disorder, the SAED pattern was measured along with the [1 1 0] zone axis. As shown in the inset of figure 1(b), one cannot find any diffraction spots with $h + k + l =$ odd such

Table 1. Structure parameters and BVS results of CCMIO refined from XRD pattern at RT[a].

Parameter	CCMIO
a (Å)	7.41060(1)
O_y	0.1732(4)
O_z	0.3034(4)
U_{iso} for Ca ($100 \times$ Å^2)	1.19(9)
U_{iso} for Cu ($100 \times$ Å^2)	0.47(2)
U_{iso} for Mn/Ir ($100 \times$ Å^2)	2.45(1)
U_{iso} for O ($100 \times$ Å^2)	0.72(8)
d_{Cu-O} (×4)	1.94203
d_{B-O} (×6)	1.97846
∠B–O–B	139.0(1)
∠Cu–O–B	109.9(1)
BVS (Cu)	2.09
R_{wp} (%)	4.95
R_p (%)	3.25

[a] Crystal data: space group *Im*-3 (No. 204); atomic sites: Ca 2a (0, 0, 0); Cu 6b (0, 0.25, 0.25); B (Mn/Ir) 8c (0.25, 0.25, 0.25); O 24h ($0, y, z$). The BVS values (V_i) were calculated using the formula $V_i = \sum_j S_{ij}$, and $S_{ij} = \exp[(r_0 - r_{ij})/0.37]$. The value of $r_0 = 1.679$ for Cu and 4 coordinated oxygen atoms were used.

as the (1 1 1) and (3 1 1) spots, revealing the absence of Mn/Ir long-range order at the B site, in agreement with the XRD result. The refined structure parameters are listed in table 1. In comparison, the lattice parameter of CCMIO (7.4106 Å) is located between those of $CaCu_3Ir_4O_{12}$ (7.4738 Å) [22] and $CaCu_3Mn_4O_{12}$ (7.2410 Å) [21], suggesting that the Mn and Ir form a solid solution. According to the refined Cu–O bond length, the bond valence sum (BVS) calculations show the valence state of Cu to be +2.09, indicating the presence of a Cu^{2+} state with square-planar coordination. Because of the random Mn/Ir arrangement, we cannot obtain the valence states for these two transition metals by BVS calculations.

The oxidation states of the Cu, Mn and Ir ions in CCMIO were investigated by x-ray absorption at the Cu-$L_{2,3}$, Mn-$L_{2,3}$ and Ir-L_3 edges, respectively. Figure 2(a) shows the Cu-$L_{2,3}$ XAS of CCMIO together with those of Cu_2O as a Cu^+ ($3d^{10}$) [28] and $CaCu_3Ti_4O_{12}$ as a Cu^{2+} ($3d^9$) [29] in a quadruple perovskite structure. Typically, for a $3d^9$ Cu^{2+} charge state, a strong absorption peak appears around 930.0 eV due to the $d^9 \rightarrow \underline{c}d^{10}$ transition [28], where $\underline{c}$ indicates a hole in the Cu 2p core. Obviously, the Cu-$L_{2,3}$ spectrum of CCMIO exhibits a very strong single peak at the same energy position as that of $CaCu_3Ti_4O_{12}$ revealing the formation of a Cu^{2+} valence state in CCMIO with a $Cu^{2+}O_4$ square-planar local environment. In comparison, the main peak of Cu_2O is shifted to higher energy by about 2.5 eV corresponding to a $d^{10} \rightarrow \underline{c}d^{10}s^1$ transition [28] of the fully occupied $3d^{10}$ configuration in Cu^+. This does not occur in CCMIO, thus excluding the Cu^+ state. Figure 2(b) shows the Mn-$L_{2,3}$ XAS spectra of CCMIO with those of the reference oxides including the tetravalent La_2MnCoO_6 (Mn^{4+}, from [30]) and the trivalent $LaMnO_3$ (Mn^{3+}, from [30]) with similar MnO_6 octahedral coordination. Compared with $LaMnO_3$, the main absorption peaks of CCMIO move towards higher energy by more than 1 eV. They have however the same energy position and similar spectral features as

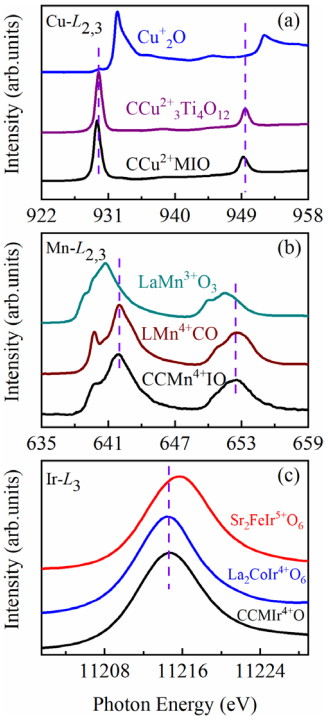

Figure 2. XAS of (a) Cu-$L_{2,3}$ edges of CCMIO and the references $CaCu_3Ti_4O_{12}$ and Cu_2O, and (b) Mn-$L_{2,3}$ edges of CCMIO and the references La_2MnCoO_6 (LMCO, from [28]) and $LaMnO_3$ (from [28]), and (c) Ir-L_3 edges of CCMIO and the references $La_2CoIr^{4+}O_6$ (from [30]) and $Sr_2FeIr^{5+}O_6$ (from [31]).

those of the Mn^{4+} reference La_2MnCoO_6. This finding indicates the presence of a Mn^{4+} ($3d^3$) state in CCMIO. The difference at the shoulder of the Mn L_3 peak might be due to the slightly different charge transfer and ligand field effects between La_2MnCoO_6 and CCMIO. The observed Mn^{4+} state in CCMIO is surprising considering the Mn^{3+} state in the $Sr_3Ru_{2-x}Mn_xO_7$ [31].

The Ir-L_3 XAS spectra of CCMIO, La_2CoIrO_6 as an Ir^{4+} reference (from [32]) and Sr_2FeIrO_6 as an Ir^{5+} reference (from [33]) are shown in figure 2(c). The Ir-L_3 of CCMIO is shifted by more than 1 eV to lower energy with respect to that of Ir^{5+} reference Sr_2FeIrO_6, but locates at the same energy as that of the Ir^{4+} reference La_2CoIrO_6 indicating the formation of Ir^{4+} valence state. Therefore, the XAS measurements confirm the charge combination to be $CaCu^{2+}_3Mn^{4+}_2Ir^{4+}_2O_{12}$. Usually, for two cations to form an ordered distribution in a perovskite structure, the charge difference between them is not less than two [34]. The identical charge states between Mn and Ir therefore explain the B-site disorder in CCMIO. In particular, for most quadruple perovskite oxides with hybridized 3d–5d elements at the B site, the 3d–5d charge discrepancy is larger than two and then they form an ordered distribution, as exampled by $CaCu_3Fe_2Re_2O_{12}$, $CaCu_3Fe_2Os_2O_{12}$, and $NaCu_3Fe_2Os_2O_{12}$ [23, 24, 35]. The current CCMIO therefore provides an exception where the 3d and 5d elements have exactly the same charge state.

The magnetism of CCMIO was studied by both dc and ac magnetizations. Figure 3(a) shows the temperature dependence of zero-field-cooling (ZFC) and field-cooling (FC) dc

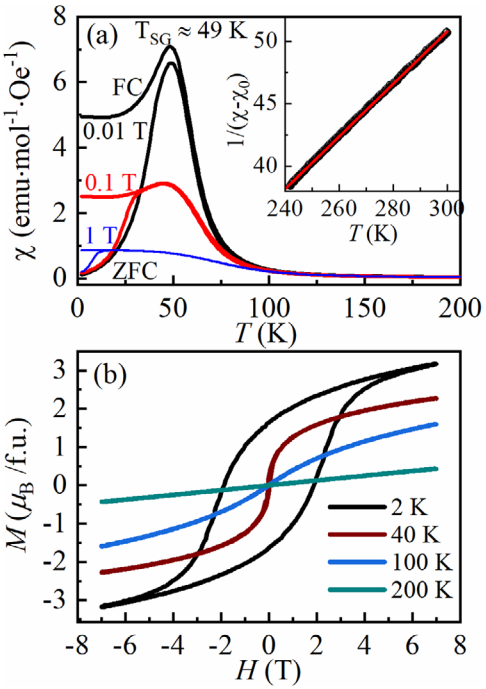

Figure 3. (a) dc magnetic susceptibility of CCMIO measured at different magnetic fields. The inset shows the Curie–Weiss fitting in 240–300 K. (b) Isothermal magnetization measured at selected temperatures.

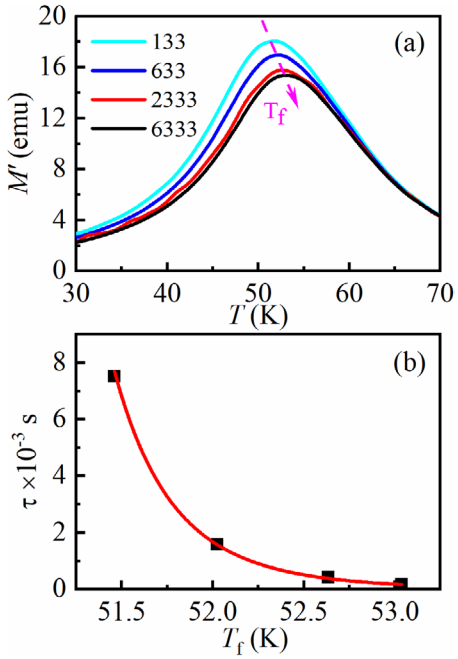

Figure 4. (a) Temperature dependence of ac magnetic susceptibility measured at different frequencies. (b) The fitted results based on the dynamic slowing down model as described in text.

magnetic susceptibility curves measured at different fields. The ZFC and FC curves separate from each other at a critical temperature $T_{SG} \approx 49$ K at 0.01 T. Moreover, the T_{SG} systematically shifts towards lower temperatures and the ZFC and FC curves tend to be overlapped with increasing magnetic field up to 1 T, accompanied by a gradual reduction in the intensity of χ_{dc} and a broadening of the cusp around T_{SG}. These features are indicative of a spin glass transition. Figure 3(b) shows the field-dependent magnetization curves measured at different temperatures. At higher temperatures like 200 K, the linear magnetization behavior is observed, as expected for the paramagnetism. At 100 K, the magnetization slightly deviates from the linear dependence on field. It may suggest the formation of some short-range FM interactions. At 2 K, one can find remarkable magnetic hysteresis with a ~2 T coercive field, but the magnetization is still not saturated with fields up to 7 T. These observations are in good agreement with the occurrence of spin glass. Above 240 K, the susceptibility data can be fitted using the modified Curie–Weiss (CW) law $\chi(T) = \chi_0 + C/(T - \theta_w)$, where χ_0 is the temperature independent term containing the core diamagnetism and Van Vleck paramagnetism [33, 36]. The inset of figure 3(a) shows the fitting results, which give a Curie constant $C = 4.75$ emu·K · mol^{-1} · Oe^{-1}, a Weiss temperature $\theta_w = 58.5$ K, and a $\chi_0 = 3.5 \times 10^{-3}$ emu · mol^{-1} · Oe^{-1}. According to the Curie constant, the effective magnetic moment is calculated to be $\mu_{eff} = (8C)^{1/2} = 6.17$ μ_B/f.u. If one only considers the spin-only contribution of Cu^{2+} and Mn^{4+} ions, the effective moment in theory is 6.24 μ_B/f.u., which is very close to the fitting one. Therefore, compared to the 3*d* Cu^{2+} and Mn^{4+}, the 5d Ir^{4+} may play a minor role on the magnetism of CCMIO. Actually, there is no long-range magnetic order occurring in the isostructural compound $CaCu_3Ir_4O_{12}$ [22].

To further clarify the spin glass behavior of CCMIO, ac magnetization was measured at different frequencies by spanning several orders of magnitude. As shown in figure 4(a), the ac magnetization shows a cusp at a spin freezing temperature T_f. Moreover, with increasing frequency, the cusp shifts toward higher temperatures with a reduction in magnitude. These features provide another convincing evidence for the occurrence of spin glass. We can characterize the shift of T_f with frequency using a physical parameter $\kappa = \Delta T_f/[T_f \Delta \ln(\omega)]$, where the spin freezing temperature T_f is determined from the maximum of M', ω is the ac frequency, and ΔT_f and $\Delta \ln(\omega)$ represent the differences for different frequencies. The κ is calculated to be about $0.8(1) \times 10^{-2}$ for CCMIO. The value of κ can offer a criterion for distinguishing a spin glass from a super-paramagnet since the later usually has a larger value of κ. For example, κ is 0.28 for the typical super-paramagnet compound a-(Ho_2O_3) (B_2O_3) [37] and 0.1 for $La_{0.67}Sr_{0.33}MnO_3$ nanoparticles [38]. The smaller κ value of CCMIO indicates that the compound should be a spin glass system rather than a super-paramagnet, as reported in other spin glasses like the magnetic B_{12} cluster compound $HoB_{22}C_2N$ [39]. In addition, the frequency dependence of T_f can be described by a conventional dynamical slowing down model for a three dimension spin glass system with the function $\tau/\tau_0 = [(T_f - T_{SG})/T_{SG}]^{-zv}$ [40]. Here, $\tau_f = 1/\omega$ corresponds to the maximum relation time of the system at T_f, τ_0 is the intrinsic relaxation time, and zv is the dynamic exponent. Figure 4(b) shows the plot of τ_f versus T_f and the fitting result, yielding $zv = 7.67$ and $\tau_0 = 8.22 \times 10^{-13}$ s. The fitted value

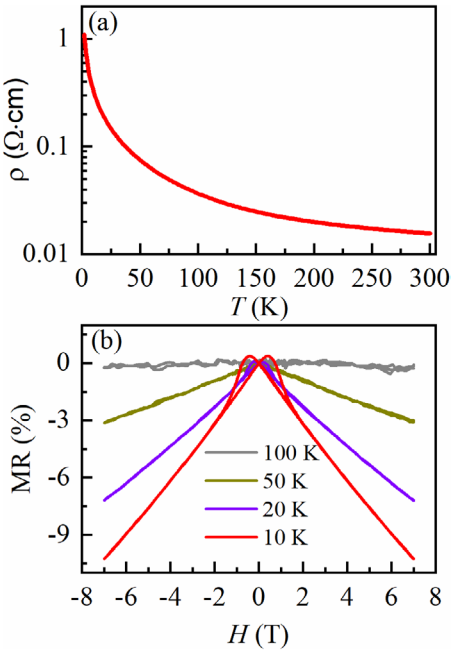

Figure 5. (a) Temperature dependence of resistivity measured on heating at zero field for CCMIO. (b) Magnetoresistance as a function of magnetic field measured at different temperatures.

of τ_0 is in accordance with the typical values of 10^{-11}–10^{-13} s obtained for many canonical spin glasses such as CuMn [37] and $Eu_{0.5}Sr_{1.5}MnO_4$ [41].

The spin glass behavior of CCMIO can be attributed to the competing FM and AFM interactions. According to the Goodenough–Kanamori rules [42, 43], for a Mn^{4+} ion with $3d^3$ configuration in a perovskite octahedral crystal field, the Mn^{4+}–O–Mn^{4+} AFM superexchange interaction is expected to occur as observed in $CaMnO_3$ [44]. On the other hand, in *A*-site ordered perovskites, the presence of a net ferromagnetic component is possible due to the $Cu^{2+}(\uparrow)Mn^{4+}(\downarrow)$ ferrimagnetic coupling, as reported in $CaCu_3Mn_4O_{12}$ [21]. In addition, for the 5*d* Ir^{4+}, the strong spin-orbital coupling splits the t_{2g} level into a fully occupied $j_{\text{eff}} = 3/2$ band and a singly occupied $j_{\text{eff}} = 1/2$ state, resulting in a total $J_{\text{eff}} = 1/2$ pseudospin state. An AFM interaction is often shown in $J_{\text{eff}} = 1/2$ systems, such as Sr_2IrO_4 and La_2CoIrO_6 [45, 46]. As for the spin interaction between the *B*-site Mn^{4+} with half-filled t_{2g} orbitals and Ir^{4+} with half-filled $j_{\text{eff}} = 1/2$ band is concerned, it most probably leads to $Mn^{4+}(\uparrow)Ir^{4+}(\downarrow)$ ferrimagnetic correlation as discussed in another 3*d*/5*d* hybridized system Pb_2FeOsO_6 [47]. Therefore, a series of complex and competing FM and AFM interactions are responsible for the spin glass behavior of CCMIO.

Based on the charge states and magnetism of the current $CaCu_3Mn_2Ir_2O_{12}$, we may discuss the magnetic evolution of $CaCu_3Mn_{4-x}Ir_xO_{12}$ solid solution. In the undoped $CaCu_3Mn_4O_{12}$, there is a long-range ferrimagnetic transition with a T_C as high as 355 K [21]. In the end member of $CaCu_3Ir_4O_{12}$, however, paramagnetic behavior is found to occur [22]. Since the B-site Mn and Ir ions have the same +4 valence state in $CaCu_3Mn_{4-x}Ir_xO_{12}$ family, the substitution of Ir cannot change the electronic configuration of Mn^{4+} (t_{2g}^3) but cause chemical disorder, so that a B-site completely disordered perovskite structure is formed in the intermediate composition of $CaCu_3Mn_2Ir_2O_{12}$. Therefore, it is expected that, with increasing Ir substitution, $CaCu_3Mn_{4-x}Ir_xO_{12}$ will change from long-range ferrimagnetic ordering to paramagnetism via an intermediate spin glass state, as illustrated by CCMIO. This is essentially different from that of the Re-doped $CaCu_3Mn_{4-x}Re_xO_{12}$ [48], in which the doped Re has a higher valence state of +6. Thus, the introduction of Re will change the initial Mn^{4+} state to be a mixed Mn^{3+}/Mn^{4+} valence state. As a result, a small amount of Re doping such as with $x = 0.1$ can significantly decreases the resistivity while the T_C is almost unchanged.

The temperature dependent resistivity and magnetoresistance effects are measured to characterize the electrical transport properties of CCMIO. As shown in figure 5(a), the resistivity measured at 300 K is only 15.6 mΩ · cm, which is slightly larger than that observed in $CaCu_3Ir_4O_{12}$ with metallic conductivity arising from the itinerant electronic behavior of Ir^{4+} ions. In CCMIO, although the resistivity lightly increases with decreasing temperature, taking into account the polycrystalline nature where the extrinsic grain boundaries play a role on electrical transport, the weak temperature dependence of resistivity (especially at higher temperatures such as above 100 K) as well as the disordered perovskite structure with itinerant Ir^{4+} state may imply a (bad) metallic electrical behavior. As presented in figure 5(b), CCMIO shows negative magnetoresistance effects $\text{MR} = 100\% \times [\rho(H) - \rho(0)]/\rho(0)$ at different temperatures. Lowering temperature can enhance the MR effects. At 10 K and 7 T, the absolute value of MR is about 10.3%, which is considerably less than that observed in the isostructural compound $CaCu_3Mn_4O_{12}$ due to the decrease of Mn^{4+} component. In comparison, a slightly Re-doping for Mn can cause the Mn^{3+}/Mn^{4+} mixed valence state, giving rise to enhanced MR effects as observed in $CaCu_3(Mn_{3.9}Re_{0.1})O_{12}$ [48].

4. Conclusions

In summary, an Ir-containing quadruple perovskite oxide $CaCu_3Mn_2Ir_2O_{12}$ was prepared at 5.5 GPa and 1673–1773 K. The Rietveld analysis based on the powder XRD data reveals an *A*-site ordered perovskite structure with space group *Im*-3, in which the Mn and Ir ions are disorderly distributed at the *B* site. The valence states and local environment of Cu, Mn and Ir were investigated by XAS techniques, giving $Cu^{2+}O_4$ square-planar coordination at the *A*′ site and $Mn^{4+}/Ir^{4+}O_6$ octahedral coordination at the *B* site, resulting in the charge combination of $CaCu_3^{2+}Mn_2^{4+}{}_2Ir_2^{4+}O_{12}$. In magnetism, both dc and ac magnetization measurements indicate a spin glass transition around a spin freezing temperature of 49 K. Moreover, the spin glass behavior can be well described by a conventional dynamic slowing down model. In comparison with the isostructural compound $CaCu_3Mn_4O_{12}$, the MR effect of the

current CCMIO is reduced considerably owing to the introduction of Ir.

Acknowledgments

This work was supported by the National Key R&D Program of China (Grant No. 2018YFA0305700, 2018YFE0103200), the National Natural Science Foundation of China (Grant No. 51772324, 11574378, 11934017), and the Chinese Academy of Sciences (Grant No. QYZDB–SSW–SLH013, GJHZ1773). The research in Dresden was partially supported by the DFG through SFB 1143. We acknowledge the support from the Max Planck-POSTECH-Hsinchu Center for Complex Phase Materials.

ORCID iDs

Youwen Long https://orcid.org/0000-0002-8587-7818

References

[1] Cava R J, Batlogg B, Vandover R B, Murphy D W, Sunshine S, Siegrist T, Remeika J P, Rietman E A, Zahurak S and Espinosa G P 1987 *Phys Rev Lett.* **58** 1676–9
[2] Wang J *et al* 2003 *Science* **299** 1719–22
[3] Kimura T, Goto T, Shintani H, Ishizaka K, Arima T and Tokura Y 2003 *Nature* **426** 55–8
[4] Salamon M B and Jaime M 2001 *Rev. Mod. Phys.* **73** 583–628
[5] Dagotto E, Hotta T and Moreo A 2001 *Phys. Rep.* **344** 1–153
[6] Jin S, Tiefel T H, Mccormack M, Fastnacht R A, Ramesh R and Chen L H 1994 *Science* **264** 413–5
[7] Mahendiran R, Tiwary S K, Raychaudhuri A K, Ramakrishnan T V, Mahesh R, Rangavittal N and Rao C N R 1996 *Phys. Rev.* B **53** 3348–58
[8] Millis A J 1996 *Phys. Rev.* B **53** 8434–41
[9] Martinelli A, Ferretti M, Castellano C, Mondelli C, Cimberle M R, Tropeano M and Ritter C 2006 *Phys. Rev.* B **73** 064423
[10] Castellano C, Ferretti M, Martinelli A and Cimberle M R 2009 *J. Alloys Compd.* **478** 479–83
[11] Long Y W, Kaneko Y, Ishiwata S, Tokunaga Y, Matsuda T, Wadati H, Tanaka Y, Shin S, Tokura Y and Taguchi Y 2012 *Phys. Rev.* B **86** 064436
[12] Long Y and Shimakawa Y 2010 *New J. Phys.* **12** 063029
[13] Long Y-W, Kawakami T, Chen W-T, Saito T, Watanuki T, Nakakura Y, Liu Q-Q, Jin C-Q and Shimakawa Y 2012 *Chem. Mater.* **24** 2235–9
[14] Shimakawa Y 2008 *Inorg. Chem.* **47** 8562–70
[15] Yin Y-Y, Wang X, Deng H-S, Zhou L, Dai J-H and Long Y-W 2017 *Acta Phys. Sin.* **66** 030201
[16] Zhou L, Wang X, Zhang H-M, Shen X-D, Dong S and Long Y-W 2018 *Acta Phys. Sin.* **67** 157505
[17] Xiang H, Liu X, Zhao E, Meng J and Wu Z 2007 *Phys. Rev.* B **76** 155103
[18] Shimakawa Y and Mizumaki M 2014 *J. Phys.: Condens. Matter* **26**
[19] Shimakawa Y and Saito T 2012 *Phys. Status Solidi* b **249** 423–34
[20] Shimakawa Y, Shiraki H and Saito T 2008 *J. Phys. Soc. Japan* **77** 113702
[21] Zeng Z, Greenblatt M, Subramanian M A and Croft M 1999 *Phys. Rev. Lett.* **82** 3164–7
[22] Cheng J G, Zhou J S, Yang Y F, Zhou H D, Matsubayashi K, Uwatoko Y, MacDonald A and Goodenough J B 2013 *Phys Rev Lett.* **111** 176403
[23] Deng H *et al* 2016 *Phys. Rev.* B **94** 024414
[24] Chen W-t, Mizumaki M, Seki H, Senn M S, Saito T, Kan D, Attfield J P and Shimakawa Y 2014 *Nat. Commun.* **5** 3909
[25] Yin Y-Y *et al* 2016 *Chem. Mater.* **28** 8988–96
[26] Kadyrova N I, Mel'nikova N V, Ustinova I S and Zainulin Y G 2016 *Inorg. Mater.* **52** 1051–4
[27] Larson A C and Dreele R B V 2004 *Los Alamos National Laboratory Report* LAUR 86-784 Los Alamos National Laboratory
[28] Tjeng L H, Chen C T and Cheong S W 1992 *Phys. Rev.* B **45** 8205–8
[29] McGuinness C, Downes J E, Sheridan P, Glans P A, Smith K E, Si W and Johnson P D 2005 *Phys. Rev.* B **71** 195111
[30] Burnus T *et al* 2008 *Phys. Rev.* B **77** 125124
[31] Hossain M A *et al* 2008 *Phys. Rev. Lett.* **101** 016404
[32] Agrestini S *et al* 2019 *Phys. Rev.* B **100** 014443
[33] Dai J H *et al* 2018 *Phys. Rev.* B **97** 085103
[34] Vasala S and Karppinen M 2015 *Prog. Solid State Chem.* **43** 1–36
[35] Wang X *et al* 2019 *Inorg. Chem.* **58** 320–6
[36] Dey T *et al* 2016 *Phys. Rev.* B **93** 014434
[37] Mydosh J A 1993 *Spin Glasses: an Experimental Introduction* (London: Taylor & Francis)
[38] Rostamnejadi A, Salamati H, Kameli P and Ahmadvand H 2009 *J. Magn. Magn. Mater.* **321** 3126–31
[39] Mori T and Mamiya H 2003 *Phys. Rev.* B **68** 214422
[40] Hohenberg P C and Halperin B I 1977 *Rev. Mod. Phys.* **49** 435–79
[41] Mathieu R, Asamitsu A, Kaneko Y, He J P and Tokura Y 2005 *Phys. Rev.* B **72** 014436
[42] Goodenough J B 1955 *Phys. Rev.* **100** 564–73
[43] Kanamori J 1959 *J. Phys. Chem. Solids* **10** 87–98
[44] Goodenough J B 1967 *Phys. Rev.* **164** 785–9
[45] Crawford M K, Subramanian M A, Harlow R L, Fernandezbaca J A, Wang Z R and Johnston D C 1994 *Phys. Rev.* B **49** 9198–201
[46] Lee S, Lee M-C, Ishikawa Y, Miao P, Torii S, Won C J, Lee K D, Hur N, Cho D-Y and Kamiyama T 2018 *Phys. Rev.* B **98** 104409
[47] Zhao Q *et al* 2016 *Inorg. Chem.* **55** 9816–21
[48] Ben Hassine R, Sanchez-Benitez J, Alonso J A, Cherif W, Mompean F J and Fernandez-Diaz M T 2017 *J. Alloys Compd.* **696** 73–8